



## Integration of highly sensitive large-area graphene-based biosensors in an automated sensing platform

Melanie Meincke<sup>a,b</sup>, Andre Bazzone<sup>a</sup>, Stephan Holzhauser<sup>a</sup>, Maria Barthmes<sup>a</sup>, Lars Richter<sup>b</sup>, Fabian Knechtel<sup>b</sup>, Evelyn Ploetz<sup>b</sup>, Michael George<sup>a</sup>, Niels Fertig<sup>a</sup>, Izabela Kamińska<sup>b</sup>, Philip Tinnefeld<sup>b,\*</sup>

<sup>a</sup> Nanion Technologies, Ganghoferstraße 70A, 80339 Munich, Germany

<sup>b</sup> Ludwig-Maximilians-Universität, Department of Chemistry, Butenandtstraße 5-13, 81377 Munich, Germany

### ARTICLE INFO

#### Keywords:

Biosensors  
SGFET  
Graphene  
SSM technology

### ABSTRACT

Graphene-based biosensors, featuring exceptional electronic, mechanical, and surface properties, have emerged as frontrunners in advanced sensing technologies. However, to achieve widespread industrial adoption, advancements in the fabrication and integration of large-area graphene devices are essential. Critical parameters such as enhanced sensitivity, scalable production methods, economic viability, integration capabilities, and consistent uniformity must be meticulously addressed. In this work, we demonstrate that our ultra-clean, chemical wet transfer protocol of large-area graphene enables a scalable, smooth integration of graphene into an established assay platform for transporter protein drug discovery. Furthermore, we demonstrate sensitive detection of electrolytic buffers, varying pH, bovine serum albumin (BSA) and single-stranded DNA (ssDNA) adsorption, using our large-area graphene solution-gated field-effect transistor (SGFET) sensors, thereby proving their robust and reliable performance. The sensors' biocompatibility and ion sensitivity, down to the picomolar range, substantiate their suitability for the investigation of electroactive transport in ion channels and membrane transporters.

### 1. Introduction

Graphene, an atomically thin carbon layer, is highly sensitive to environmental changes, including biomolecular interactions and charge transfer [18]. This sensitivity arises from its outstanding surface-to-volume ratio and tuneable electron mobility in response to the adsorption of charged moieties [31]. Conventional fabrication techniques for micron-scale graphene sensors have been costly and challenging to implement in industrial settings, limiting their widespread adoption. [31,30]. The production of graphene via chemical vapour deposition (CVD) on copper foil, followed by its clean transfer onto a substrate of interest, has advanced the development of graphene transistors and sensing devices considerably [28,17]. This innovation has paved the way for using large-area graphene in the manufacturing of biosensors with enhanced sensitivity and reduced detection limits. Such improvements allow for the accurate detection of target trace analytes even in complex samples [10]. Despite these advancements, significant potential remains in the application of graphene's ultra-high conductivity and

low resistivity to enhance automated pipetting platforms tailored for electrophysiological experiments. This manuscript aims to bridge this gap by integrating large-area graphene sensors into an existing solid-supported membrane technology. The integration of graphene significantly enhances the capability of this platform to conduct ion-sensitive measurements at a high-throughput level, enabling rapid detection of multiple analytes [7]. This is vital for advancing sensor technology in fields where reliability and stability are highly important, such as biotechnology, healthcare, environmental monitoring, and food safety [35,19]. By implementing a wet-chemical transfer protocol for CVD-grown graphene, we realize graphene-based biosensors and explore their feedback to various analytes and different conditions, including changes in ion strength and concentration, as well as the adsorption of protein and ssDNA. Sodium and potassium ions are here only two of many agents, which play major roles in membrane transport events. Our investigations not only highlight the practical application of graphene sensors in an industrial setting but also pave the way for their broader adoption across different scientific domains, setting a cornerstone for

\* Corresponding author.

E-mail address: [philip.tinnefeld@cup.uni-muenchen.de](mailto:philip.tinnefeld@cup.uni-muenchen.de) (P. Tinnefeld).

<https://doi.org/10.1016/j.measurement.2024.115592>

Received 10 June 2024; Received in revised form 8 August 2024; Accepted 23 August 2024

Available online 28 August 2024

0263-2241/© 2024 The Author(s). Published by Elsevier Ltd. This is an open access article under the CC BY license (<http://creativecommons.org/licenses/by/4.0/>).

future technological and methodological innovations in sensor technology.

### 1.1. Graphene field-effect transistors

Graphene field-effect transistors (GFETs) enable highly sensitive detection of electroactive molecules [27,32]. An ideal, defect-free graphene surface can neither be protonized, nor deprotonated and is therefore insensitive to electrolytic solutions. Charge transfer between graphene and solutes predominantly occurs at the edges of graphene or defects in its basal plane [12]. An extensive surface area of graphene frequently harbours a wealth of defects, resulting in numerous electroactive sites [25]. When the target substrate interacts with the surface, changes in the electric charge distribution occur, thereby influencing the charge carrier density at the recognition layer and consequently the conductivity of the channel connecting the source and drain electrodes [10,22]. This interplay of substrate-surface interaction, charge carrier density and the conductivity of the channel forms the scientific foundation underpinning our approach to sensor design and operation.

### 1.2. Solution-gated field-effect transistors

Solution-gated field-effect transistors (SGFETs) have captured considerable attention due to their utility in sensor applications [22,15]. Distinguished from conventional field-effect transistors, SGFETs incorporate a reference electrode, increasing the sensitivity to changes at the electrolyte-semiconductor interface [20]. Their ability to host numerous electroactive sites and enhanced sensitivity to changes in the charge environment provide a convenient method to improve FET biosensor performance [29,4]. This has paved the way for sensing applications in fields such as DNA profiling [24,33,13,6] and glucose detection [34,5,36], not only advancing biomedical sensing but also presenting opportunities in gas, light and pressure sensing [35].

### 1.3. Measurement setup

The proposed graphene sensing system is based on a semi-automated pipetting platform from Nanion Technologies [2,3]. The sensor is built as a SGFET with three metal electrodes (Fig. 1A). The substitution of a conventional gate with a reference electrode, effectively renders the threshold voltage responsive to the interfacial potential at both, the

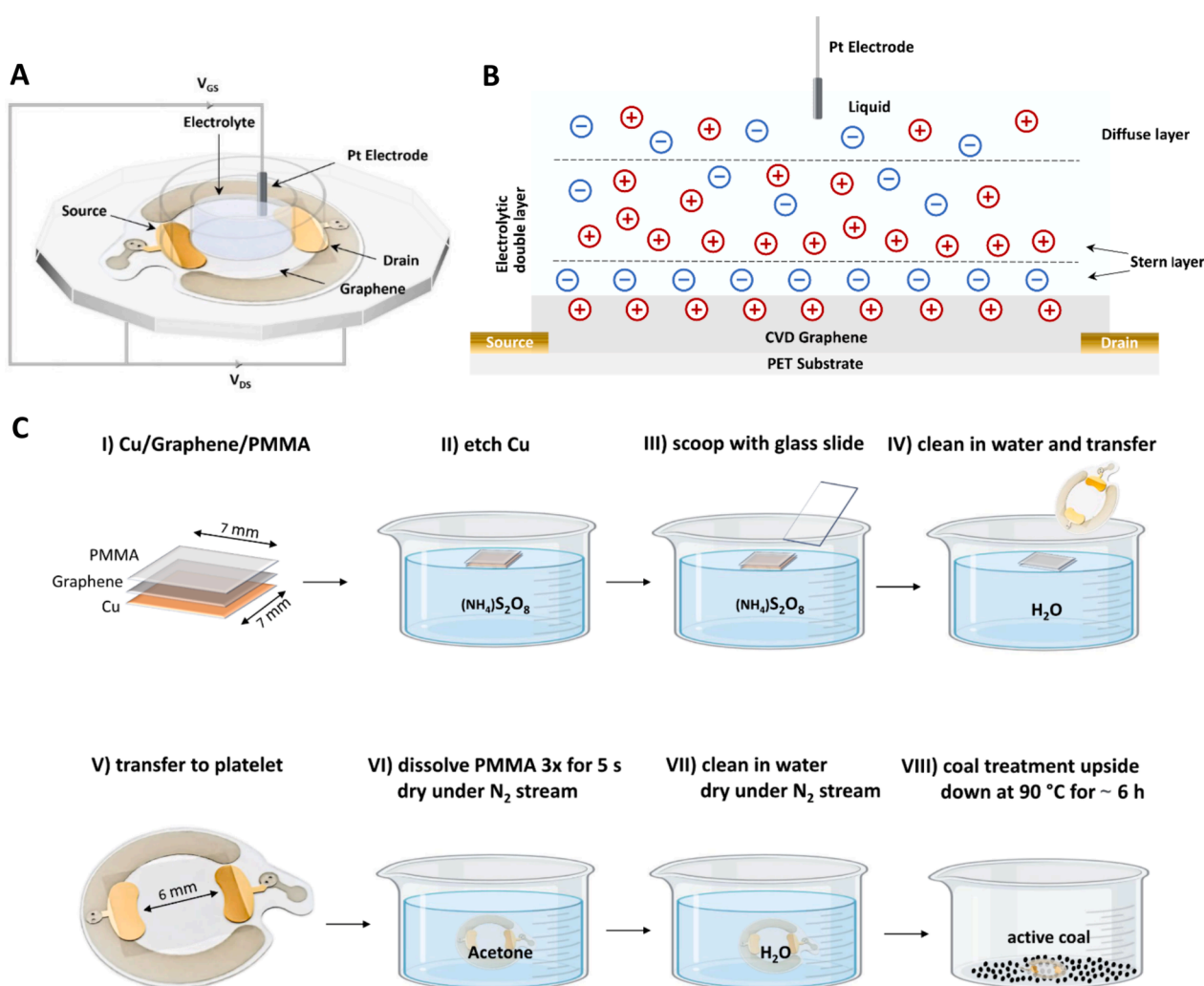


**Fig. 1.** Basic architecture of the graphene-based solution-gated field-effect transistor with its electrolytic double layer model and the fabrication process. A) The experimental setup includes the source and drain electrodes, which are connected by a graphene monolayer, featuring an electronic channel between the two electrodes. Additionally, a platinum top gate electrode is immersed in the electrolyte. B) Electrolytic double layer model of the graphene-based SGFET setup, featuring the three-electrode setup with graphene as the channel connecting the source and the drain electrodes on a polyethylene terephthalate (PET) substrate. The third electrode is immersed in the electrolyte. C) Preparation process from PMMA graphene copper foil sample to PET substrate which is further glued into a plastic casing to isolate the source and the drain from the solution.

electrolyte-gate and the electrolyte-semiconductor interface. Any changes in the interfacial potential, therefore, result in a discernible shift in the semiconductor's conductance. The I-V characterisation process involves the measurement of the drain-source current  $I_{DS}$  for a constant drain-source voltage  $V_{DS}$  while varying the gate voltage  $V_{GS}$ . The efficacy of modulating the source-drain current by manipulating the gate voltage is given by the transconductance ( $g_m$ ), defined as the derivative of the  $I_{DS}$ - $V_{GS}$  transfer curve. The transconductance is directly proportional to both the electron mobility of the graphene layer and the interfacial capacitance. Characterisation of the transconductance allows for the evaluation of the charge neutrality point (CNP), which is commonly known as the Dirac point [15]. The CNP is strictly related to graphene's doping and the electrochemical potential of the reference electrode. Due to the electron-hole symmetry of graphene, the underlying sensor exhibits ambipolar transfer characteristics, indicating that the device features p-channel (hole conduction) behaviour at the negative gate voltage side and n-channel (electron conduction) behaviour at the positive gate voltage side for a given source/drain voltage. In the case of p-doped graphene, the CNP shifts towards more positive values of  $V_{GS}$ , whereas for n-doped graphene, it shifts to more negative values. When graphene is immersed in a polarizable electrolyte, it behaves almost equivalent to an ideal polarizable electrode, especially in an electrolyte without any redox species [15,9]. In SGFET experiments, the graphene-electrolyte interface can be modelled as a combination of two capacitors in series: the quantum capacitance and the electrolytic double layer (EDL) capacitance [15]. The first layer of the EDL consists of ions with opposite charges to those present in the polarizable graphene electrode, while the second layer consists of ions with positive and negative charges that progressively reach the potential of the solution far from the electrode (Fig. 1B). At the CNP, the quantum capacitance reaches its minimum, because the density of states in graphene is at its lowest. The low quantum capacitance results in minimal conduction and forms the bottom of the characteristic V-shape in an SGFET experiment [15]. As the gate voltage moves away from the CNP, the EDL capacitance surpasses the quantum capacitance, which increases the total capacitance and enables the addition of more charge carriers. This results in an increased conductance, forming the arms of the V-shape observed in the output graph.

## 2. Materials and methods

The sensor chips were prepared using a  $7 \times 7 \text{ mm}^2$  piece of polyethylene terephthalate (PET) with 50 nm gold source/drain electrodes on the top side and printed silver electrodes on the bottom side. The sensor platelets were acquired from Conductive Technologies Inc. Prior to the transfer of graphene, the substrates were cleaned with acetone and dried under a gentle nitrogen stream. A polymethylmethacrylate (PMMA)/graphene/copper foil from Graphenea® was cut into  $7 \times 7 \text{ mm}^2$  pieces and transferred to float on the surface of a 0.2 M ammonium persulfate solution for etching of the copper from the back side for 4 h. The graphene with PMMA on top was scooped with a clean glass coverslip and the graphene was released to a beaker with MilliQ water to wash off the residual ammonium persulfate. The washed graphene sample was then scooped with the clean PET substrate in an orientation that allows contacting of the two gold electrodes on the top side (see Fig. 1C). After annealing overnight, the PMMA was removed by cleaning the platelets three times for five seconds in acetone and subsequently, the platelets were dried under a gentle nitrogen stream. Next, the platelets were dipped into water once for five seconds and dried again under a gentle nitrogen stream. The thus prepared samples were heated on active coal for several hours at 90 °C. The whole workflow is portrayed in Fig. 1C. The average two-point resistance of the sensors ( $n = 50$ ) in air without an electrolyte gate was  $1.7 \pm 0.25 \text{ k}\Omega$ , which indicates the uniformity of the devices' production process. For comparison, Graphenea® advertises a sheet resistance for their graphene on PET of  $0.58 \pm 0.05 \text{ k}\Omega/\text{sq}$ . The resistance values are highly dependent on the

underlying substrate, the transfer process, and the cleaning steps. A table with the sheet resistance values can be found in the [supporting material \(SI Table 1\)](#). This data together with the IV-curves of different devices (SI Fig 1) on 1 M KCl ( $n = 9$ ) at  $V_{DS}=0.1 \text{ V}$  which exhibit a CNP at  $0.21 \pm 0.08 \text{ V}$  give access to the stability and the reproducibility of the sensing devices. The source and drain electrodes are isolated from the electrolyte by a plastic casing to prevent high gate leakage currents and unstable device performance when a gate voltage is applied. A photograph of the sensor platelet before PMMA removal and after gluing it into the plastic casing is depicted in Fig. 2A–C. The graphene surface and the PET chip were characterized by brightfield imaging and raman mapping (SI Fig. 2) to monitor the chemical composition and flatness. Specifications for the raman characterization are provided in the [supporting information](#). Additionally, the laser scanning microscope image in Fig. 2D shows the homogeneity of the graphene sheet and its orientation on the source and the drain nodes. For all measurements, the sensors were positioned in a faraday cage (Fig. 2E) to facilitate electrical contact of the source and the drain from the bottom side. The solution exchange was executed by a semi-automated pipetting robot, the SURFE<sup>2</sup>R N1 instrument, provided by Nanion Technologies (Fig. 2F). The SURFE<sup>2</sup>R is a well-established instrument for solid supported membrane based electrophysiology (SSME) commonly used for membrane transporter analysis [2]. A customized software was developed for the measurements, enabling precise control over various parameters. These include the modulation of gate voltage, source/drain voltage, gain, number of samples, sampling rate, step size, and intervals between the steps. The application of gate voltage is accomplished through a platinum reference electrode, which is immersed in the electrolyte (Fig. 2E). Adjusting the gate voltage causes a modulation of the charge carrier density in graphene and thus the channel's conductance.

## 3. Results and discussion

Graphene transferred onto PET exhibits p-doped characteristics, as is usually observed for graphene grown by CVD [14]. This accounts for the observed shift of the CNP towards positive gate voltages (approximately 0.2 V) in 1 M KCl with an applied  $V_{DS}$  of 0.1 V (see Fig. 3A). Increased source-drain voltages promoted an additional displacement of the CNP of  $53.0 \pm 1.5 \text{ mV}$  per 100 mV increment (inc) towards higher gate voltages, which is visualized in Fig. 3B. It is noteworthy that this shift remains constant in the hole conduction branch, as illustrated in Fig. 3A. In the electron conduction branch, a change in transconductance is observed due to the increasing charge accumulation on the sensor surface, which affects electron mobility. This change is influenced by the ionic strength of the solution. The influence of the ionic strength on  $I_{DS}$  is detailed in the study by Purwidyantri et al. [26]. For the following measurements the  $V_{DS}$  was set at a constant 100 mV. Further specifications of measurement parameters are described in the [supporting information](#). Different sensors reveal slight variations, such as in their CNP and transconductance yet exhibit comparable properties with a shift of the CNP of  $46.7 \pm 6,0 \text{ mV}$  per 100 mV ( $n = 3$ ). When a graphene SGFET is immersed in a solution containing sodium ions, the adsorption of sodium ions on the graphene surface induces an alteration in the local electrostatic potential, thereby influencing the distribution of charge within the graphene layer. This gives rise to a shift of the Dirac point, which results in a variation of the electrical current flowing through the SGFET. Therefore, the  $V_{GS}$  of the CNP is used for quantifying ion concentrations as depicted in Fig. 3C for the detection of sodium chloride over a dynamic range from picomolar to molar. Besides the position of the CNP, also the shapes of the IV-curves change for varying sodium chloride concentrations (Fig. 3C). This is related to the change of transconductance caused by the increase of the capacity of the EDL with higher ion concentrations [26]. SGFET measurements may therefore be employed for the precise detection and quantification of sodium ion concentration in a designated electrolyte [11].

For our concentration gradient measurements, we applied different

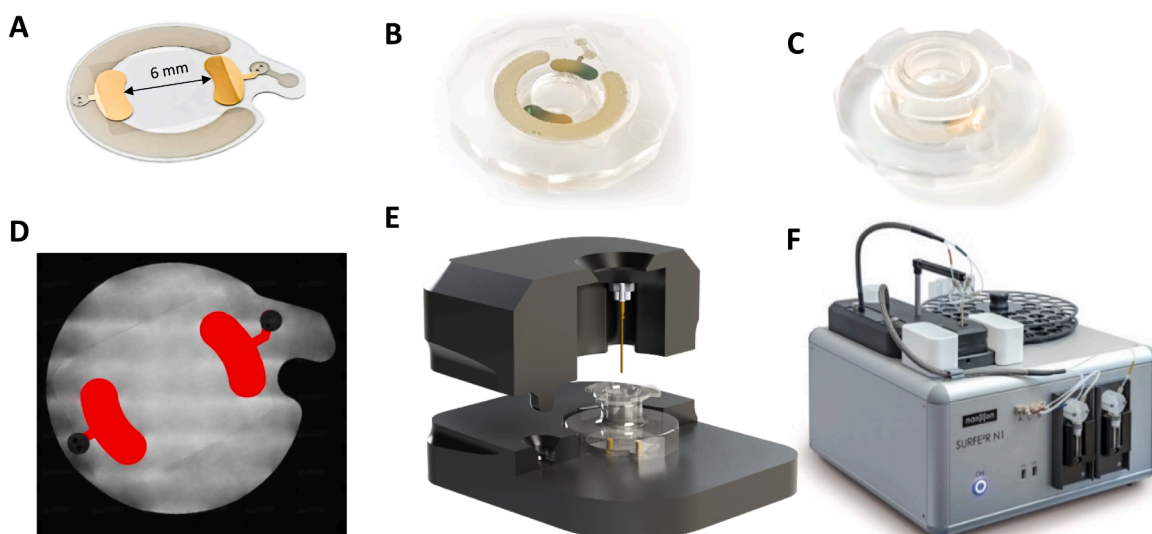


**Fig. 2.** Assembly of the sensor substrate, optical image of the platelet and embedment into the sensing platform. A) Photograph of PET platelet with PMMA coated graphene sample on it and the ready-to-use sensor with plastic casing from B) lower and C) upper view. D) Image of the platelet with graphene on it under the laser scanning microscope. E) The sensors are placed in a faraday cage to assure low noise measurements. 3-D model with a cut through the measurement chamber. The nodes for electrical contacting of the source, drain and the gate electrode are depicted in golden color. F) The solution exchange is performed with a semi-automated pipetting technology.

concentrations of electrolytic buffers with an automated pipetting robot onto the graphene surface. The so-called Ion Jet enables rapid exchange of the solutions using a pre-installed rinsing protocol [2,3]. Between the measurements, the well was rinsed thoroughly with 1 mL of the buffer containing the respective sodium chloride concentration. Fig. 3C depicts the shift of the Dirac point in response to varying concentrations of sodium chloride. Plotting the Dirac points as a function of sodium concentration as shown in Fig. 3D gives access to the device's sensitivity (80 mV/dec). Similarly, the plots for potassium concentrations were obtained (SI Fig. 3), ranging from  $10^{-1}$  M down to  $10^{-10}$  M, yielding a sensitivity of 90 mV per decade and a limit of detection (LOD) of  $10^{-10}$  M. Table 1 lists a comparison of recent graphene-based ion-sensitive sensors in the literature, demonstrating the competitiveness of our sensors to existing technologies. Apart from the acquisition of IV-curves under constant source/drain current voltage and variable gate voltage conditions, our experimental setup allows for continuous, real-time measurements. Real-time measurements were carried out for varying potassium concentrations under a source/drain voltage of 100 mV and a gate voltage of 50 mV (Fig. 3E). Changes of salt concentration are reflected by stepwise increase of the source/drain current, as expected from the IV-curves (analogous data for potassium chloride in SI Fig. 3). Fig. 3E also provides insight into decreased ion concentrations, which correlate with an enhanced drift in the source/drain current. A plausible explanation for this phenomenon is the reduced prominence of the EDL in the diluted solutions [12]. As a result, the impact of surface defects on the graphene becomes more conspicuous in lower-concentrated electrolyte solutions. A marginal reduction in the source/drain current upon solution exchange can, furthermore, be attributed to the rapid solution exchange on the sensing surface and a transient perturbation of the EDL. Apart from a shift of the Dirac point with a change in ion concentration, the ion strength can induce a change in the transconductance. We demonstrate this by applying phosphate buffer (PB) at different concentrations and a constant concentration of 10 mM varying the pH from 5 to 9 (Fig. 4A). Previous studies conducted by Mailly-Giacchetti et al. demonstrated the suitability of PET as a substrate for graphene-based pH sensing in solution [21]. Their results revealed the electrical response of SGFET devices that remain neither affected by the specific substrate to which graphene is transferred nor the presence of fabrication-related organic residues atop the graphene surface. Their findings provide

evidence that the pH sensing mechanism is primarily governed by an electronic charging effect of the EDL, which arises from the adsorption of hydroxyl and hydronium ions on the graphene surface. The ambipolar characteristics of both hydroxyl ( $\text{OH}^-$ ) and hydroxonium ( $\text{H}_3\text{O}^+$ ) ions facilitate a modulation of the channel conductance by doping with either holes or electrons. The charge transfer mechanism is contingent on the ions which are specifically bound at the inner Helmholtz plane at the graphene/electrolyte interface, as elucidated by Ang et al. [1]. The adsorption of hydronium ions ( $\text{H}_3\text{O}^+$ ), hydroxyl ( $\text{OH}^-$ ) and other surface ions would accordingly follow a non-faradaic, capacitive process. This assumption implies that charge carriers are unable to transmit across the graphene/solution interface. Consequently, an elevated presence of hydroxonium ions at the graphene/electrolyte interface would leave the graphene n-doped, whereas the existence of hydroxyl ions confers to p-doping. A higher pH, therefore, leads to a higher accumulation of hydroxyl ions on the sensing surface. This, in turn, induces an alteration in the local charge carrier concentration within the graphene channel, leading to a rightward shift of the Dirac point as seen in its electrical conductance behaviour. The magnitude of this Dirac point shift (Fig. 4A–B) exhibits a sensitivity of 24 mV per pH unit. In contrast, an elevated concentration of PB (Fig. 4C–D) at the same pH leads to a shift of the Dirac point to more n-doped regions. While the hole branch to the left of the Dirac point demonstrates minimal transconductance variations, the conduction branch to the right of the Dirac point exhibits substantial changes with increasing PB concentration. This asymmetry is primarily due to the varying ionic strength, which affects the Debye length and hence the screening of electric fields by mobile ions near the graphene surface. In solutions with high ionic strength severe charge screening effects can be observed, which reduce the sensitivity of the SGFET to changes in ion concentration [8]. To evaluate the compatibility of our sensors with biological substrates, we additionally investigated the response of our GSFETs to BSA and ssDNA. When a graphene-based SGFET is functionalized with a protein such as BSA, the protein molecules can adsorb onto the surface of the graphene and modify its electronic properties. BSA is a protein that is commonly used as a blocking agent to prevent nonspecific binding in biosensor applications. It has an isoelectric point ranging from pH 5.1 to 5.5 bearing an overall negatively charged character at pH 7 [23]. Due to its net negative charge at neutral pH, BSA can induce a local electrostatic potential. This local

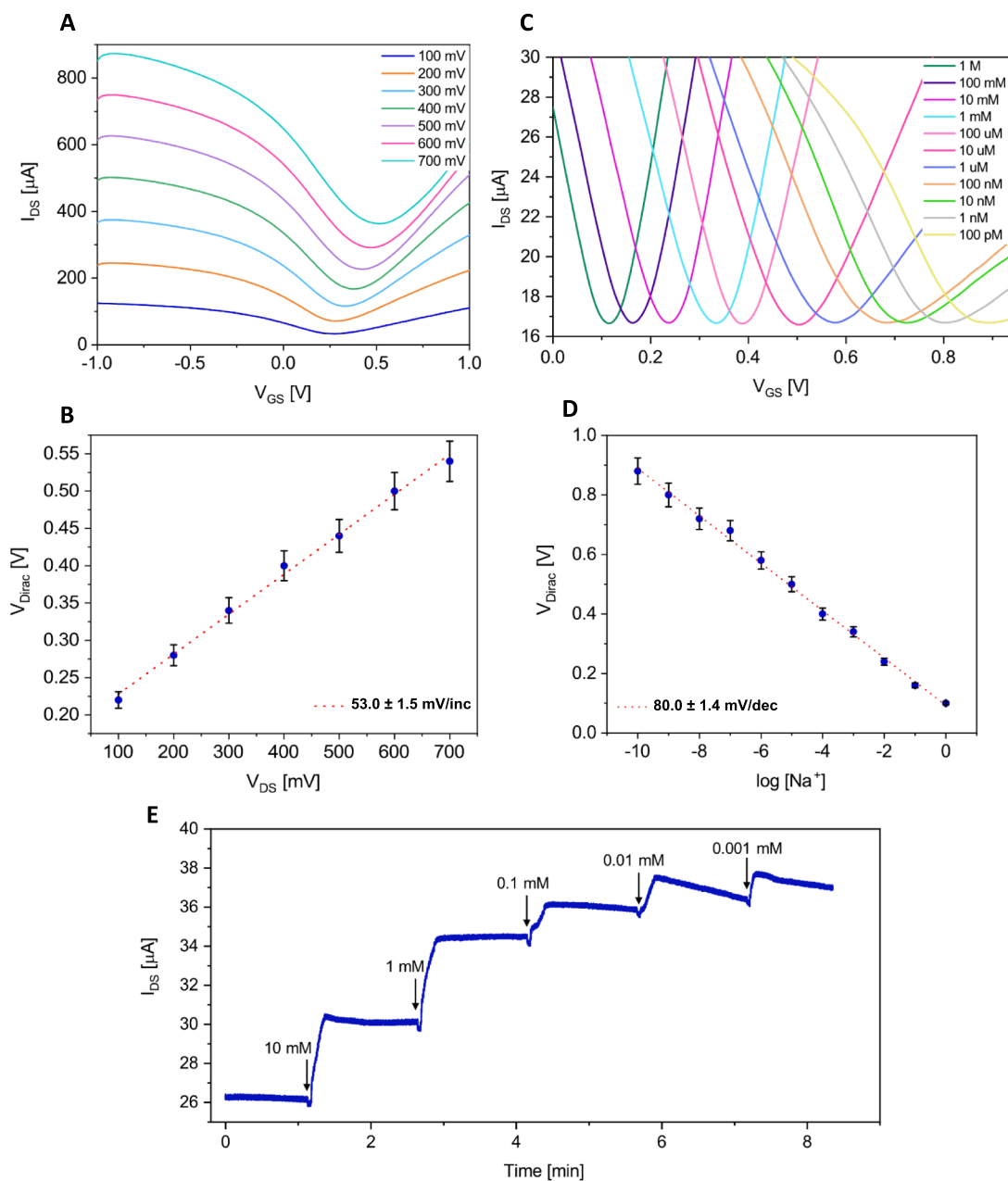


**Fig. 3.** Gate voltage sweep curves, the linear fit of the Dirac point and real-time measurement with the SURFE<sup>2</sup>R pipetting robot A)  $I/V$  curves for  $V_{DS}$  varying between 100 and 700 mV. B)  $V_{Dirac}$  for  $V_{DS}$  from 100 to 700 mV and the respective linear fit. C)  $I/V$  curves for the sodium chloride concentrations ranging from 1 M to 100 pM at a  $V_{DS}$  of 100 mV. D) Linear fit of  $V_{Dirac}$  for concentrations ranging from 1 M to 100 pM at a constant source/drain voltage of 100 mV. E) Real-time acquisition of the well rinsing at constant 50 mV gate voltage with a KCl solution of the respective concentration starting from 100 mM down to 0.001 mM. The source/drain current increases with lower concentrations. A slight drop in current with application of the solution can be attributed to the rapid solution exchange on the surface and the re-establishment of the dynamic equilibrium.

electrostatic potential creates a repulsive force on electrons, pushing them away from the surface of graphene. This effect leads to an effective increase of positive charge carriers in the graphene (holes). As a result, more positive gate voltage is required to balance the excess holes and reach the CNP. This leads to a CNP shift to the right towards more positive gate voltages as BSA concentration increases (Fig. 5A–B). A comparison of recent BSA sensors in literature can be found in SI Table 2. Apart from BSA, we also observed the response of our sensors to the adsorption of ssDNA. ssDNA is a negatively charged molecule due to its phosphate backbone. However, when ssDNA adsorbs onto the graphene surface, it does not induce hole doping like BSA. Instead, the ssDNA's negative charges provide additional electron density to the graphene. The adsorption of ssDNA can, therefore, result in electron accumulation

near the graphene surface or in the regions it interacts with, effectively creating an n-doping effect [4]. Therefore, less positive gate voltage is required to reach the CNP, which causes a shift of the CNP towards more negative gate voltages. Consequently, the increased electron density leads to a decrease in the source-drain voltage required to drive a current, as the graphene becomes more conductive with more available charge carriers. In Fig. 5C and D, we highlighted this consequence. An increased concentration of ssDNA leads to a shift of the CNP to more negative gate voltages and decreased source-drain voltages.

#### 4. Conclusion

In conclusion, our graphene-based sensors enhance the utility of the

**Table 1**  
Comparison of recent graphene-based ion-sensitive sensors in literature.

Reference	Device	Active area	Ionic Sensitivity	LOD (M)	
Na <sup>+</sup>	This work	PET/Graphene	~0.6 cm <sup>2</sup>	80 mV/dec	10 <sup>-10</sup>
	[16]	SiO <sub>2</sub> /Graphene/ISM	~0.5 nm <sup>2</sup>	152.4 mV/dec	10 <sup>-8</sup>
	[11]	SiO <sub>2</sub> , parylene C /Graphene/ISM	~0.4 cm <sup>2</sup>	49.2 mV/dec	10 <sup>-6</sup>
K <sup>+</sup>	This work	PET/Graphene	~0.6 cm <sup>2</sup>	90 mV/dec	10 <sup>-10</sup>
	[11]	SiO <sub>2</sub> , parylene C /Graphene/ISM	~0.4 cm <sup>2</sup>	45.7 mV/dec	~10 <sup>-5</sup>
	[10]	SiO <sub>2</sub> , parylene C /Graphene/ISM	~0.4 cm <sup>2</sup>	37 mV/dec	10 <sup>-9</sup>

SURFE<sup>2</sup>R device beyond capacitive measurements. Solution-gated ion-sensitive measurements facilitated by graphene's tunable surface properties allow for a differentiated approach to understanding ionic interactions at the biosensor interface. We demonstrate this through real-time IV-current measurements with potassium chloride. Our results showcase the sensor's outstanding sensitivity, increased LOD for several orders of magnitude in comparison to previous findings, stability, and resilience under challenging environments (e.g. rapid solution exchange under varying pH). Using graphene's optimal charge neutrality and quantum capacitance, we exploit interfacial properties to enhance sensor performance significantly. The system's benefit is highlighted by its ability to amplify sensor sensitivity, enabling the precise detection of

subtle electrical signal fluctuations. The integration of a PET substrate into our graphene sensor platform provides reproducible signals and enhances cost-effectiveness, making our sensors economically viable and scalable. The integration of graphene into the SSME technology from Nanion Technologies, additionally, addresses a significant limitation of this device which will be addressed in future experiments — the requirement to detach cells and disrupt them in their native state for measurements. Our graphene-based sensors facilitate direct culturing of cells or cell membrane fragment measurements on the biocompatible graphene surface, maintaining their physiological integrity and providing more reliable data reflective of their natural biological states. Our results also suggest the potential for our graphene sensors to improve the signal-to-noise ratio compared to traditional gold sensors in capacitive measurements. This enhancement is critical for resolving previously indiscernible kinetics due to poor signal-to-noise ratios, potentially allowing for a deeper understanding of transporter behaviours and interactions in future studies. For these experiments, the surface will be functionalized with a lipid monolayer which will, additionally, prohibit unspecific binding of charged molecules from the buffer. Selectivity can be introduced in membrane transporter measurements by use of cells or cell membrane fragments which are genetically modified to only express a certain transporter. Overall, this innovative sensor technology not only holds promise for rapid real-time detection of electroactive molecules but also for the specific detection of membrane transport activities. With the potential to monitor transient currents both via capacitive measurement approaches and direct current readouts from real-time graphene sensing experiments, our system exemplifies the successful implementation of large-area graphene into

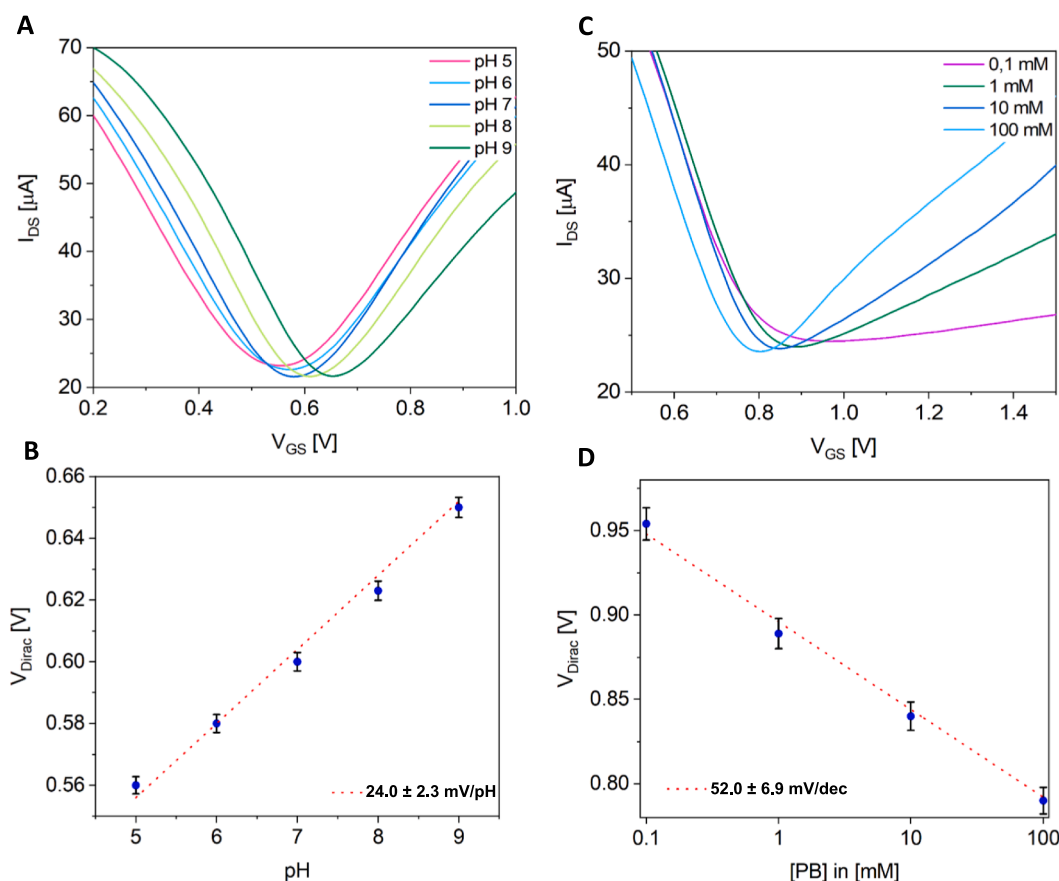


**Fig. 4.** I/V curves and linear fit of the Dirac point for varying pH values of 10 mM PB and varying concentrations of PB at pH 7. A) I/V curves for 10 mM phosphate buffer at pH 5 to 9. An increase of the pH causes a shift of the Dirac point to higher gate voltages. B) Linear fit of the voltage at the Dirac point against the applied phosphate buffer solutions with their pH ranging from 5 to 9. The Dirac point increases proportionally with the pH of the phosphate buffer. C) I/V curves for different phosphate buffer concentrations 0.1 to 100 mM. D) Linear fit of the voltage at the Dirac point against the applied phosphate buffer solutions with concentrations ranging from 0.1 to 100 mM.

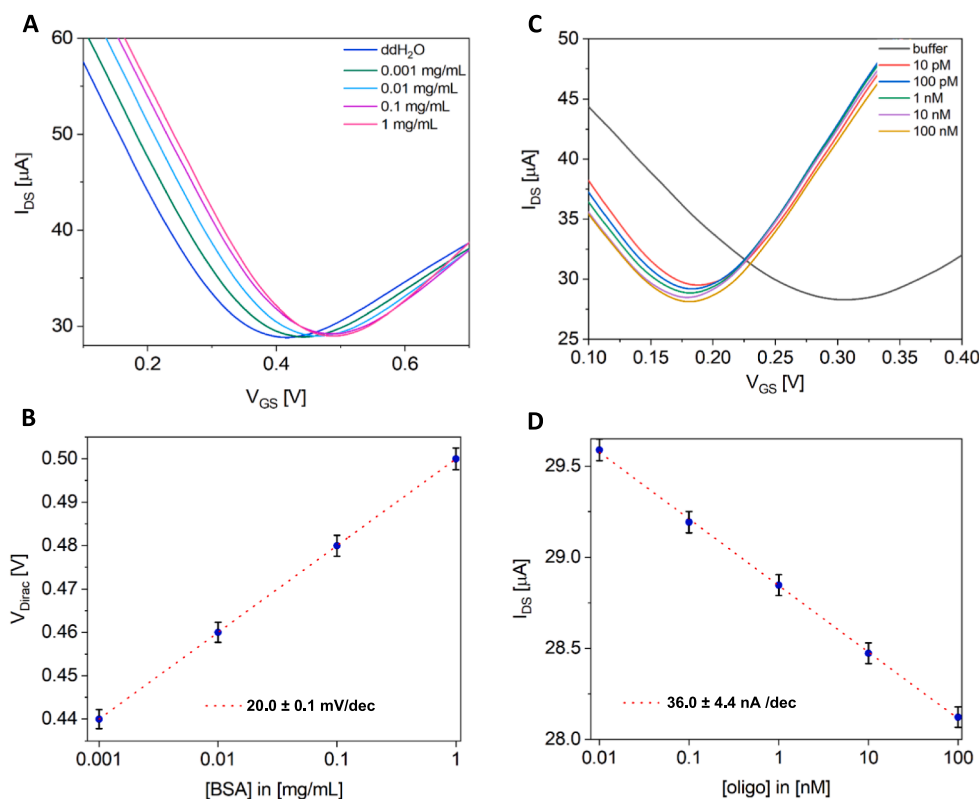


**Fig. 5.** I/V curves and linear fit of the Dirac point for varying BSA and DNA concentration. A) I/V curves for different BSA concentrations 0.001 to 1 mg/mL. B) Linear fit of the voltage at the Dirac point of the curves against the applied BSA solutions with concentrations ranging from 0.001 to 1 mg/mL. The increase of the Dirac point with higher BSA concentrations is directly related to the increase of the protein concentration. C) I/V curves for different oligo concentrations from 10 pM to 100 nM. D) Linear fit of the source drain current at the Dirac point 0.18 mV of all curves against the oligonucleotide concentrations ranging from 10 pM to 100 nM.

existing industrial technology.

#### CRediT authorship contribution statement

**Melanie Meincke:** Writing – review & editing, Writing – original draft, Validation, Project administration, Methodology, Investigation, Funding acquisition, Formal analysis. **Andre Bazzone:** Writing – review & editing, Supervision. **Stephan Holzhauser:** Software, Resources. **Maria Barthmes:** Writing – review & editing, Methodology. **Lars Richter:** Writing – review & editing, Methodology. **Fabian Knechtel:** Methodology. **Evelyn Ploetz:** Formal analysis, Writing – review & editing. **Michael George:** Writing – review & editing, Project administration. **Niels Fertig:** Writing – review & editing, Project administration. **Izabela Kamińska:** Writing – review & editing, Methodology. **Philip Tinnfeld:** Writing – review & editing, Supervision, Project administration, Conceptualization.

#### Declaration of competing interest

The authors declare the following financial interests/personal relationships which may be considered as potential competing interests: [Melanie Meincke reports financial support was provided by LMU Munich Center for Nanoscience. Melanie Meincke reports financial support was provided by Cusanuswerk Sponsorship Organization for Gifted Students. Melanie Meincke reports a relationship with Nanion Technologies GmbH that includes: non-financial support. If there are other authors, they declare that they have no known competing financial interests or personal relationships that could have appeared to influence the work reported in this paper].

#### Data availability

Data will be made available on request.

#### Acknowledgements

The project in cooperation of the Ludwig-Maximilians-University (LMU) and Nanion Technologies was kindly funded by the Center for NanoScience (CeNS), the LMU and the Cusanuswerk.

#### Appendix A. Supplementary material

Supplementary material to this article can be found online at <https://doi.org/10.1016/j.measurement.2024.115592>.

#### References

- [1] P.K. Ang, W. Chen, A.T.S. Wee, K.P. Loh, Solution-gated epitaxial graphene as pH sensor, *J. Am. Chem. Soc.* 130 (44) (2008) 14392–14393.
- [2] A. Bazzone, M. Barthmes, K. Fendler, SSM-based electrophysiology for transporter research, *Methods Enzymol.* 594 (2017) 31–83.
- [3] A. Bazzone, A. Körner, M. Meincke, M. Bhatt, S. Dondapati, M. Barthmes, et al., SSM-based electrophysiology, a label-free real-time method reveals sugar binding & transport events in SGLT1, *Biosens. Bioelectron.* 197 (2022) 113763.
- [4] A. Béraud, M. Sauvage, C.M. Bazán, M. Tje, A. Bencherif, D. Bouilly, Graphene field-effect transistors as bioanalytical sensors: Design, operation and performance, *Analyst* 146 (2) (2021) 403–428.
- [5] A. Cagang, I.H. Abidi, A. Tyagi, J. Hu, F. Xu, T.J. Lu, Z. Luo, Graphene-based field effect transistor in two-dimensional paper networks, *Analytica Chimica Acta* 917 (2016) 101–106.
- [6] R. Campos, J. Borme, J.R. Guerreiro, J.G. Machado, M.F. Cerqueira, D. Y. Petrovykh, P. Alpuim, Attomolar label-free detection of DNA hybridization with electrolyte-gated graphene field-effect transistors, *ACS Sens.* 4 (2) (2019) 286–293.
- [7] N. Chauhan, T. Maekawa, D.N.S. Kumar, Graphene based biosensors—Accelerating medical diagnostics to new-dimensions, *J. Mater. Res.* 32 (15) (2017) 2860–2882.

- [8] H. Chen, X. Zhao, Z. Xi, Y.e. Zhang, H. Li, Z. Li, et al., A new biosensor detection system to overcome the Debye screening effect: dialysis-silicon nanowire field effect transistor, *Int. J. Nanomed.* (2019) 2985–2993.
- [9] M. Dankerl, M.V. Hauf, A. Lippert, L.H. Hess, S. Birner, I.D. Sharp, et al., Graphene solution-gated field-effect transistor array for sensing applications, *Adv. Funct. Mater.* 20 (18) (2010) 3117–3124.
- [10] I. Fakih, A. Centeno, A. Zurutuza, B. Ghaddab, M. Sijaj, T. Szkopek, High resolution potassium sensing with large-area graphene field-effect transistors, *Sens. Actuat. b: Chem.* 291 (2019) 89–95.
- [11] I. Fakih, O. Durnan, F. Mahvash, I. Napal, A. Centeno, A. Zurutuza, et al., Selective ion sensing with high resolution large area graphene field effect transistor arrays, *Nat. Commun.* 11 (1) (2020) 3226.
- [12] W. Fu, C. Nef, O. Knopfmacher, A. Tarasov, M. Weiss, M. Calame, C. Schönenberger, Graphene transistors are insensitive to pH changes in solution, *Nano Lett.* 11 (9) (2011) 3597–3600.
- [13] Z. Gao, H. Xia, J. Zauberman, M. Tomaiuolo, J. Ping, Q. Zhang, et al., Detection of sub-fM DNA with target recycling and self-assembly amplification on graphene field-effect biosensors, *Nano Lett.* 18 (6) (2018) 3509–3515.
- [14] S. Goniszewski, M. Adabi, O. Shaforost, S.M. Hanham, L. Hao, N. Klein, Correlation of p-doping in CVD Graphene with Substrate Surface Charges, *Scient. Rep.* 6 (1) (2016) 22858.
- [15] C. Hébert, E. Masvidal-Codina, A. Suarez-Perez, A.B. Calia, G. Piret, R. Garcia-Cortadella, et al., Flexible graphene solution-gated field-effect transistors: efficient transducers for micro-electrocorticography, *Adv. Funct. Mater.* 28 (12) (2018) 1703976.
- [16] T. Huang, K.K. Yeung, J. Li, H. Sun, M.M. Alam, Z. Gao, Graphene-based ion-selective field-effect transistor for sodium sensing, *Nanomaterials* 12 (15) (2022) 2620.
- [17] S. Krause, E. Ploetz, J. Bohlen, P. Schuler, R. Yaadav, F. Selbach, et al., Graphene-on-glass preparation and cleaning methods characterized by single-molecule DNA origami fluorescent probes and raman spectroscopy, *ACS Nano* 15 (4) (2021) 6430–6438.
- [18] Z. Li, W. Zhang, F. Xing, Graphene optical biosensors, *Int. J. Mol. Sci.* 20 (10) (2019) 2461.
- [19] Y. Luo, M.R. Abidian, J.-H. Ahn, D. Akinwande, A.M. Andrews, M. Antonietti, et al., Technology roadmap for flexible sensors, *ACS Nano* 17 (6) (2023) 5211–5295.
- [20] C. Mackin, L.H. Hess, A. Hsu, Y.i. Song, J. Kong, J.A. Garrido, T. Palacios, A current–voltage model for graphene electrolyte-gated field-effect transistors, *IEEE Trans. Electron Devices* 61 (12) (2014) 3971–3977.
- [21] B. Maily-Giacchetti, A. Hsu, H. Wang, V. Vinciguerra, F. Pappalardo, L. Occhipinti, et al., pH sensing properties of graphene solution-gated field-effect transistors, *J. Appl. Phys.* 114 (8) (2013) 084505.
- [22] Y. Ohno, K. Maehashi, Y. Yamashiro, K. Matsumoto, Electrolyte-gated graphene field-effect transistors for detecting pH and protein adsorption, *Nano Lett.* 9 (9) (2009) 3318–3322.
- [23] H.T.M. Phan, S. Bartelt-Hunt, K.B. Rodenhausen, M. Schubert, J.C. Bartz, Investigation of bovine serum albumin (BSA) attachment onto self-assembled monolayers (SAMs) using combinatorial quartz crystal microbalance with dissipation (QCM-D) and spectroscopic ellipsometry (SE), *PLoS One* 10 (10) (2015) e0141282.
- [24] J. Ping, R. Vishnubhotla, A. Vrudhula, A.C. Johnson, Scalable production of high-sensitivity, label-free DNA biosensors based on back-gated graphene field effect transistors, *ACS Nano* 10 (9) (2016) 8700–8704.
- [25] M. Pumera, Graphene in Biosensing, *Mater. Today* 14 (7–8) (2011) 308–315.
- [26] A. Purwidyantri, T. Domingues, J. Borme, J.R. Guerreiro, A. Ipatov, C.M. Abreu, Influence of the electrolyte salt concentration on DNA detection with graphene transistors, *Biosensors* 11 (1) (2021) 24.
- [27] D. Shahdeo, A. Roberts, N. Abbineni, S. Gandhi, Graphene based sensors, *Compr. Anal. Chem.* 91 (2020) 175–199.
- [28] J.W. Suk, A. Kitt, C.W. Magnuson, Y. Hao, S. Ahmed, J. An, et al., Transfer of CVD-grown monolayer graphene onto arbitrary substrates, *ACS Nano* 5 (9) (2011) 6916–6924.
- [29] P. Suvarnaphaet, S. Pechprasarn, Graphene-based materials for biosensors: a review, *Sensors* 17 (10) (2017) 2161.
- [30] S.K. Tiwari, R.K. Mishra, S.K. Ha, A. Huczko, Evolution of graphene oxide and graphene: from imagination to industrialization, *ChemNanoMat* 4 (7) (2018) 598–620.
- [31] S.K. Tiwari, S. Sahoo, N. Wang, A. Huczko, Graphene research and their outputs: Status and prospect, *J. Sci.: Adv. Mater. Devices* 5 (1) (2020) 10–29.
- [32] G. Vinodha, L. Cindrella, P.D. Shima, Graphene oxide based highly sensitive electrochemical sensor for detection of environmental pollutants and biomolecules, *Mater. Res. Exp.* 6 (8) (2019) 85548.
- [33] S. Xu, S. Jiang, C. Zhang, W. Yue, Y. Zou, G. Wang, et al., Ultrasensitive label-free detection of DNA hybridization by sapphire-based graphene field-effect transistor biosensor, *Appl. Surf. Sci.* 427 (2018) 1114–1119.
- [34] X. You, J.J. Pak, Graphene-based field effect transistor enzymatic glucose biosensor using silk protein for enzyme immobilization and device substrate, *Sens. Actuat. b: Chem.* 202 (2014) 1357–1365.
- [35] X. Zhang, Q. Jing, S. Ao, G.F. Schneider, D. Kireev, Z. Zhang, W. Fu, Ultrasensitive field-effect biosensors enabled by the unique electronic properties of graphene, *Small* 16 (15) (2020) 1902820.
- [36] Y. Zhu, Y. Hao, E.A. Adogla, J. Yan, D. Li, K. Xu, et al., A graphene-based affinity nanosensor for detection of low-charge and low-molecular-weight molecules, *Nanoscale* 8 (11) (2016) 5815–5819.